

Report on benchmark results from SCHISM

Required by: NTHMP Model validation workshop (March 30-April 1, 2011)

Prepared by: Y. Joseph Zhang, Ph.D. (VIMS)

Nov 2024

Team: Virginia Institute of Marine Science and Oregon Department of Geology & Mineral Industries (DOGAMI)

Geographic area: Oregon

1. Introduction

The state of Oregon is part of the US Pacific Northwest (PNW) region with extensive coastline and vibrant coastal communities. The primary tsunami hazards posed to these communities come from the seismic sources including both local (Cascadia Subduction Zone – CSZ) and distant sources; tsunamis generated by submarine landslides are presently not considered by DOGAMI but could be evaluated as part of future work. Current funding from NTHMP has enabled us to apply state-of-the-art technology, i.e. new geological and computational models, the latter based on unstructured grids, to remap the entire Oregon coast for both local and remote sources (Priest, 2013). Since we focused on seismic tsunamis, the tsunami propagation and inundation model we used (SELFE) was carefully benchmarked for this purpose (NTHMP, 2012; Horillo et al., 2014).

We have been working in partnership with DOGAMI in the preparation and dissemination of inundation maps since the 1990s, first under Oregon Senate Bill379, when the author (Zhang) was with OHSU, and then later after the author moved to Virginia Institute of Marine Science (VIMS). In 2011, the original model (SELFE) was benchmarked and approved by NTHMP via an NTHMP sponsored tsunami benchmarking workshop. Since then, the model has been renamed SCHISM due to license issues and has also been improved. Although SCHISM has not been formally benchmarked for inundation, SCHISM was evaluated as part of the NTHMP tsunami currents benchmarking workshop held in Portland, Oregon in 2015 and successfully passed those tests (Zhang et al., 2016; Lynett et al., 2017). Since then, SCHISM has been used by the State of Oregon to simulate tsunami inundation in select Oregon ports and harbors for the purposes of developing maritime guidance (e.g., Allan et al., 2018, 2020, 2024). Of note, these studies evaluated the interaction of fluctuating (dynamic) tides, river discharge, tsunami and variable bottom friction in order to simulate conditions that are probably closer to reality. The model was also used to remap tsunami inundation in two Oregon coast counties in order to correct for errors identified in the source DEMs (Allan et al., 2021).

This report documents the re-benchmark results using SCHISM. Since the inundation scheme of SCHISM is the same as in SELFE, and other parts of the model have been improved, it's not surprising that similar (or better) results are obtained with SCHISM, as shown below. Nevertheless, there are differences and these are not unexpected since we are not using the exact same unstructured grids as was used originally when benchmarking SELFE, because most of those files have been lost due to disk failure.

2. Model description

The fault dislocation model we use for the CSZ earthquakes is based on Okada's point source model but with extensive geophysical constraints (Priest et al., 2009; Witter et al., 2011). In our modeling of Oregon Coast tsunami inundation, we developed 15 megathrust rupture models for Cascadia subduction zone earthquakes that define vertical seafloor deformation used to simulate tsunami inundation. All of the rupture models reflected full-margin scenarios, where the entire 1,000 km long (along-strike) megathrust is considered to fail. The types of rupture models (down-dip) considered included slip partitioned to a splay fault in the accretionary wedge and models that varied the updip limit of slip on a buried (deep and shallow scenarios) megathrust fault. Coseismic slip was estimated from turbidite paleoseismic records (Goldfinger et al., 2010) and constrained from tsunami simulations at Bradley Lake (Witter et al., 2012). Alternative earthquake source scenarios were evaluated using a logic tree that ranked model performance based on geophysical and geological data. Scenario weights at the branch ends of the logic tree are the products of the weights of the two parameters, earthquake size and fault geometry, and represent the relative confidence that a particular model represents a reasonable rupture scenario based on geological and geophysical data, theoretical models and the judgment of the scientific team (Witter et al., 2011). The basal (and most important) branch of the logic tree, estimated fault slip from recurrence interval, is based on the frequency of turbidite interevent times over the last 10,000 years. The second branch of the logic tree developed for Oregon considered three rupture geometries that vary the distribution of slip on the updip end of the locked zone: (1) activation of a shallow splay fault in the accretionary wedge; (2) shallow buried rupture that tapers slip to zero at the deformation front; and (3) a deeper buried rupture that tapers slip to zero beneath a sharp break in the slope of the accretionary wedge offshore Washington and northern Oregon.

For remote sources the scientific team limited themselves to the Alaska-Aleutian subduction zone as historically it poses the most severe threat to the Oregon coast. We considered two scenarios: the 1964 Great Alaska earthquake and a hypothetical worst-case scenario. The source model for the 1964 event came from Johnson et al. (1996) while the source model for the worst-case scenario was originally used in a pilot study at Seaside, Oregon (TPSWG, 2006). Both scenarios involve $M_w \sim 9.2$ earthquakes near the eastern end of the Aleutian Islands. Results of simulations for the 1964 tsunami were checked against historical observations of water levels and wave runup along the Oregon coast, allowing verification of the hydrodynamic model (Zhang et al., 2011a).

The worst-case Gulf of Alaska earthquake scenario, identified as "Source 3" in Table 1 of Gonzalez et al. (2009), has uniform slip on 12 subfaults with each subfault assigned an individual slip value of 15, 20, 25 or 30 m. These extreme parameters result in maximum seafloor uplift nearly twice as large as uplift produced by the 1964 earthquake estimated by Johnson et al. (1996). Analyses of the maximum tsunami amplitude simulated for this source indicate beams of high energy directed toward the Oregon coast compared with other Alaska-Aleutian subduction zone sources (TPSWG, 2006). Because of its precedent use for the Seaside tsunami study by TPSWG (2006), Witter et al (2011) adopted the hypothetical Gulf of Alaska scenario as a maximum distant tsunami source for Oregon. Testing the geological plausibility of this scenario was beyond the scope of this study and remains an option for future probabilistic tsunami hazard analysis work underway for Oregon, Washington and Northern California.

The tsunami propagation and inundation model we tested in this report is SCHISM (Zhang and Baptista 2008a; Zhang et al. 2016), which was envisioned at its inception to be an open-source community-supported 3D hydrodynamic/hydraulic model. This philosophy has been the cornerstone of the model to this day. Originally developed as SELFE to address the challenging 3D

baroclinic circulation in the Columba River estuary, it has since been adopted by 400+ groups around the world and evolved into a major modeling system encompassing such physical/biological processes as general circulation (Burla et al. 2010), tsunami- and hurricane-induced compound flooding (Ye et al. 2020), ecology and water quality (Rodrigues et al. 2009ab), sediment transport (Pinto et al. 2011), wave-current interaction (Roland et al. 2011) and oil spill (Azvedo et al. 2009). Currently we maintain a central web site dedicated to this model (schism.wiki), a user mailing list and mail archive system, organize annual user group meetings since 2004 and conduct several online and in-person training courses for users.

The rapid growth of the SELFE/SCHISM user community owes a great deal to the numerical scheme used, which combines numerical accuracy with efficiency and robustness; the last two model traits are indispensable for large-scale practical applications as commonly found in tsunami hazard mitigation studies. The time stepping is done *semi-implicitly* for the momentum and continuity equations, and together with the Eulerian-Lagrangian method (ELM) for the treatment of the advection, the most stringent stability conditions for the shallow-water equations (e.g. CFL) are bypassed. The remaining stability conditions are related to the horizontal viscosity and baroclinic gradient terms, which contribution is insignificant (in the case of tsunami applications, these conditions are absent). The use of unstructured (hybrid triangular-quadrangular) grids in the horizontal dimension further enhances the model efficiency and flexibility due to their superior capability in fitting complex coastal boundary and resolving bathymetric and topographic features as well coastal structures. The vertical grid used in SCHISM (for 3D model) uses a hybridized system called LSC², which has been well demonstrated to be superior to either Z- or s-coordinates (Zhang et al. 2016). The model can be configured in multiple ways: 2D or 3D or even partially 2D/3D; Cartesian (i.e. map projection) or spherical (latitude/longitude). In tsunami applications, we typically apply the 2D hydrostatic (non-dispersive) configuration for maximum efficiency. For seismic tsunamis, we also explicitly model the earthquake stage (i.e. with moving bed) in order to obtain accurate initial acceleration (Zhang and Baptista 2008b).

The inundation algorithm in SCHISM is the same as in SELFE and uses a simple iterative procedure to capture the moving shoreline as shown in Figure 1. Because a semi-implicit scheme is used, which enables exceptionally large time step, the iterative procedure allows wetting and drying over multiple layers of elements over a single time step (i.e. with local CFL number >1). This simple procedure has led to accurate and stable results even near the wet/dry front where supercritical flow is not uncommon.

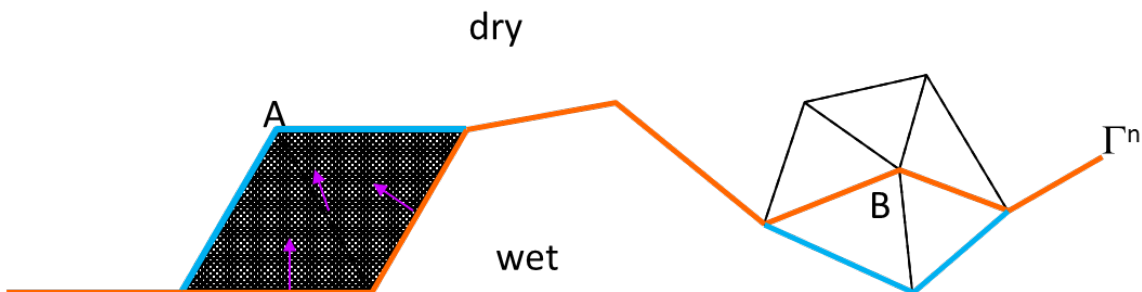


Figure 1. Inundation algorithm in SCHISM. The orange line is the shoreline from the previous time step, and the cyan lines are corrections made to obtain the shoreline at the new time step because points A is inundated, and B is dried.

The version used in this study (v5.11.0) does not explicitly model wave breaking effects, and therefore breaking waves are often represented as shock fronts in the model results. This approach is consistent with the conservative approach we apply in inundation mapping.

Since 2007 all components of the SELFE/SCHISM modeling system have been fully parallelized using domain decomposition and Message Passing Interface (MPI). This has further enhanced efficiency. For example, in the simulation of the impact of 1964 Alaska event on US west coast, we used a large grid (with 2.9 million nodes and 6 million elements) to resolve 12 major estuaries and rivers in the PNW (Zhang et al. 2011a). With 256 CPUs on NASA’s Pleiades cluster, the 6-hour simulation took only 2.25 hours of wall-clock time. This performance has since been improved by ~10-fold on newer clusters.

3. Benchmark result

As mentioned previously, we only report here the results for those benchmark problems relevant to seismic sources. We will omit a few additional cases that were originally presented for SELFE benchmarking in Zhang et al. (2011b) since they are not required by NTHMP. The benchmark tests re-examined here are fully described in the NTHMP (2012) report and summarized in Horillo et al. (2014). Following the procedures described in NTHMP (2012) and in the [NTHMP MMS guidance on model benchmarking](#), we evaluated five main tests adopted by NTHMP modeling participants. These included the following:

- BP1 (single wave on a simple beach)
- BP4 (solitary wave on a simple beach)
- BP6 (solitary wave on a conical island)
- BP7 (for tsunami runup onto a complex 3-dimensional beach at Monai Valley in lab scale)
- BP9 (Okushiri Island Tsunami).

In addition to the four NTHMP tests, we also simulated BP2 (analytical solution for solitary wave on a composite beach). More detailed descriptions of the various benchmark tests and allowable errors are fully described in Sections 1.5 to 1.9 in NTHMP (2012).

3.1 BP1: Solitary wave on simple beach – analytical solution

This canonical problem deals with a single solitary wave propagating along a constant depth and then over a sloping beach (Figure 2). The problem is completely defined by 3 parameters: d (offshore depth), β (beach slope) and H (height of the solitary wave over constant depth), and all variables are non-dimensionalized with respect to d . The goal is to validate the model for both propagation and inundation on the beach.

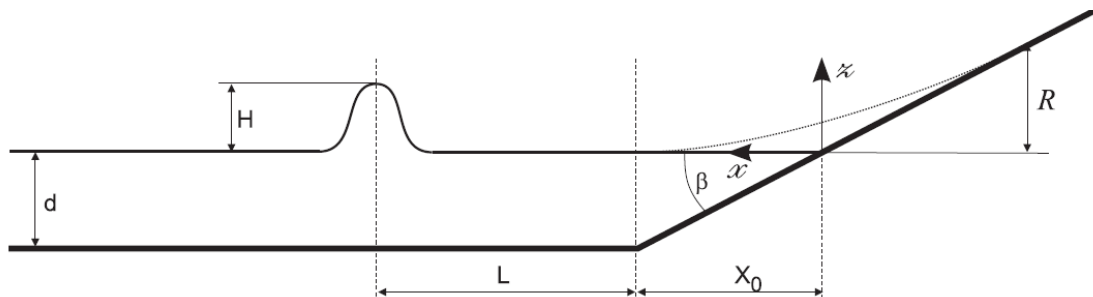


Figure 2. Domain sketch for BP1.

For convenience, we chose $d=9.81\text{m}$ in the model simulations. The model grid covers $-98\text{m} \leq x \leq 686.7\text{m}$, with 2-element wide in the y direction. A “uniform” grid with $\Delta x=\Delta y=0.1*d$ was used with each square divided into 2 triangular elements, and therefore there are altogether 2403 nodes in the grid. The time step was set at $\Delta t=0.05\text{ s}$, and the implicitness factor (in the implicit scheme) at 0.6 (the maximum runup is somewhat sensitive to this factor; as explained in Zhang and Baptista (2008b), the best accuracy is achieved near 0.5). On the left boundary a Flather type open boundary condition was imposed to minimize reflection there. We used frictionless bottom and nonlinear shallow-water equation (SWE) in order to be consistent with the assumptions made in the analytical solution.

The comparisons were made in several ways. First the surface profiles at multiple times are compared in Figure 3. The model is able to accurately simulate the entire runup and run-down process, and the performance is similar to SELFE (Table 1).

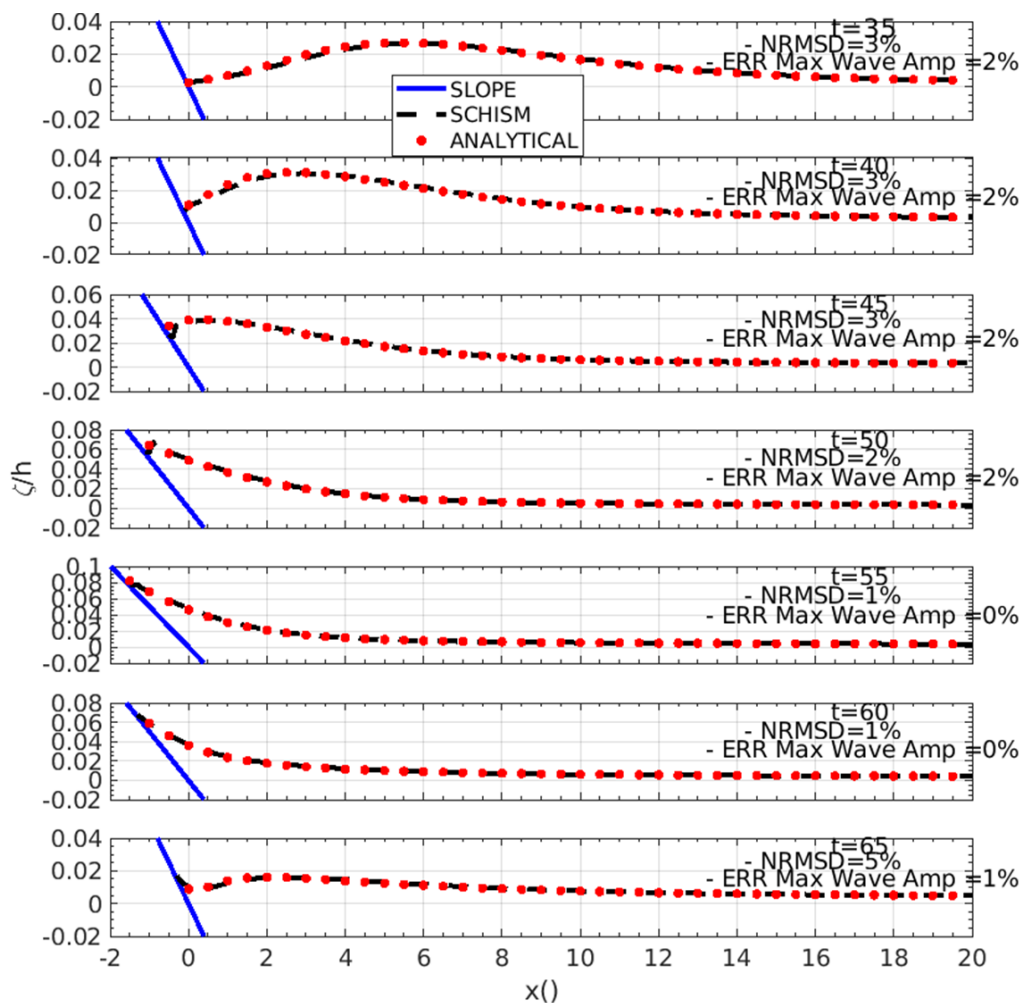


Figure 3. Comparison of surface profiles at various times for the non-breaking wave, case A ($H/d=0.0185$) of BP1. All variables have been non-dimensionalized. The RMSE at $t=60$ (near the maximum runup) is 0.001 and the Willmott skill is 0.998 (we have restricted the calculation of errors to $x<2$ to remove the uninteresting part of the solution offshore).

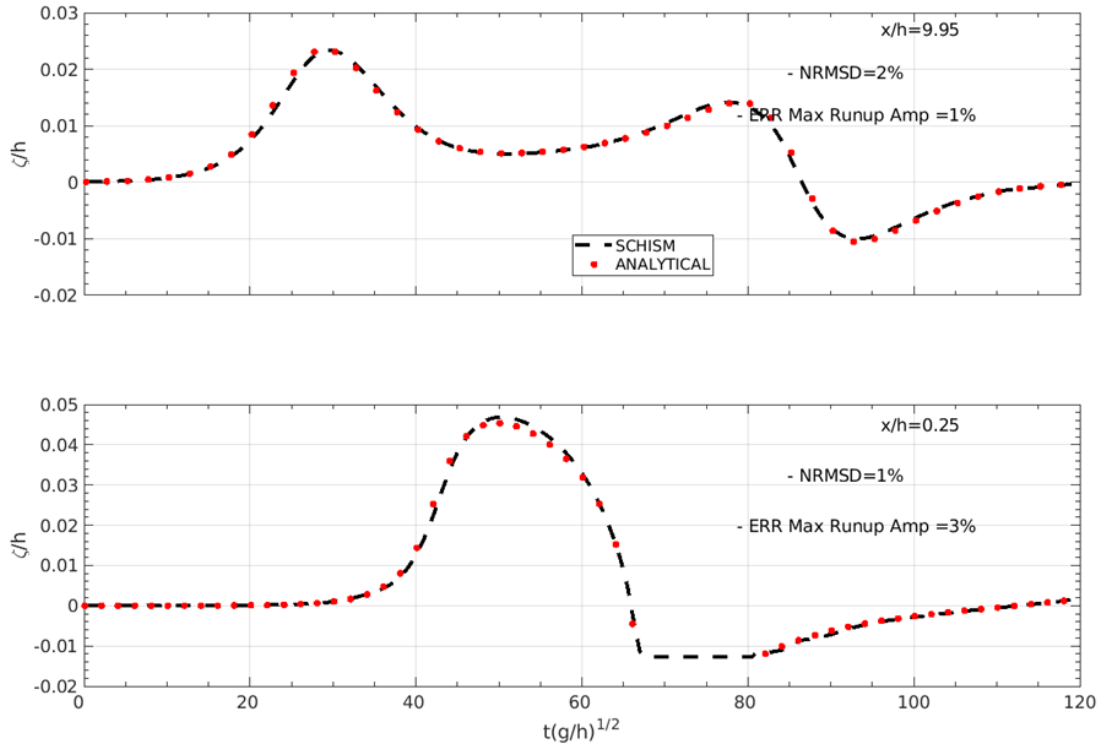


Figure 4. Comparison of elevation time series at two locations for BP1. The RMSE at the two stations are 0.001 and 0.0008, and the Willmott skill are 0.995 and 0.999, respectively.

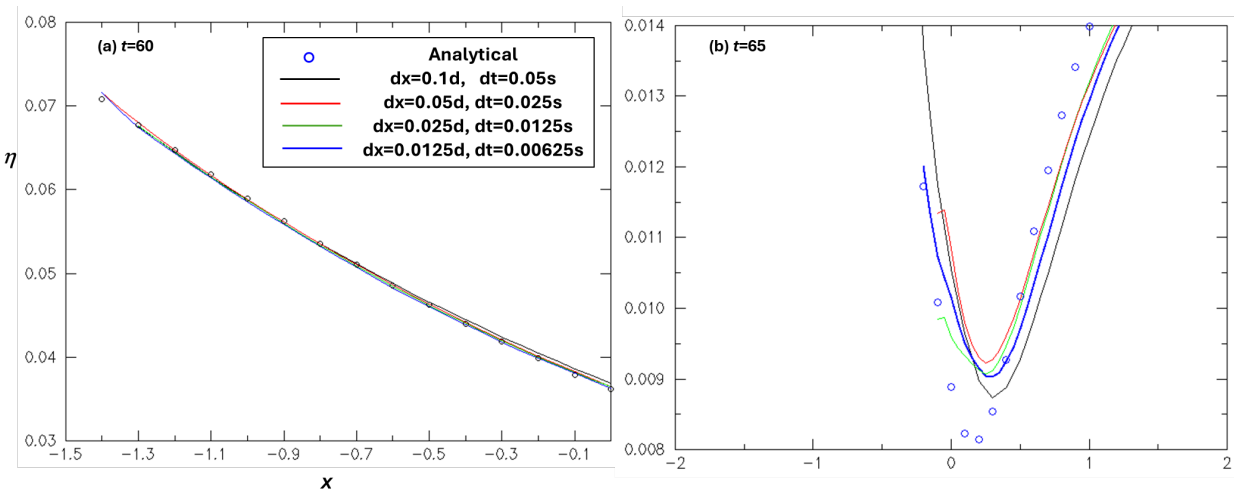


Figure 5. Convergence test for case A of BP1 at a time near (a) the maximum runup ($t=60$); (b) rundown ($t=65$).

Table 1. BP1 model errors for surface profiles at $t = [35, 40, 45, 50, 55, 60, 65]$, with respect to the analytical solution for $H/d=0.0185$, as simulated by SELFE and SCHISM. ‘RMS’ is the RMSE normalized by the data range. ‘Max’ refers to the % error at the maximum runup.

Model	t=35		t=40		t=45		t=50		t=55		t=60		t=65		Mean	
	RMS %	Max %														
SELFE	3	4	3	4	2	3	1	2	1	0	1	0	5	1	2	2
SCHISM	3	2	3	2	3	2	2	2	1	0	1	0	5	1	3	1

In addition to the conventional root-mean-square error (RMSE) we also used the Willmott skill number which is defined as (Willmott et al. 1985):

$$W = 1 - \frac{\sum (m - o)^2}{\sum [|m - \bar{o}| + |o - \bar{o}|]^2} \quad (1)$$

where m and o are model and data respectively and \bar{o} is the data mean. This number combines the contributions from both RMSE and the correlation; a Wilmot number of 1 indicates perfect skill and the model is more skilled with a higher W .

Secondly, the time series at two stations were compared (Figure 4). Note that at one station ($x=0.25$) wetting and drying occurred as indicated in both the model results and the analytical solution. Again, the model skill is high in this aspect (Table 2).

Table 2. BP1 model errors at two stations ($x = 9.95$ and $x = 0.25$) with respect to the analytical solution for $H/d= 0.0185$, as simulated by SELFE and SCHISM.

Model	x = 9.95		x = 0.25		Mean	
	RMS %	MAX %	RMS %	MAX %	RMS %	MAX %
SELFE	2	2	1	1	2	2
SCHISM	2	1	1	3	2	2

The convergence of the model is illustrated by using successively finer grid size and time step; the grid size and time step were varied in such a way that the CFL number remains constant as required by the model (Zhang and Baptista 2008a). As shown in Figure 5a, the modeled maximum runup indeed converges to the analytical value; at the finest resolution the error for the runup value is 1%. The convergence for the rundown is less good (Fig. 5b), with the error for the $t=65$ of 10% at the finest resolution (at the request and help from a reviewer, we managed to recover the analytical data at the maximum rundown at $t=70$, and the maximum rundown error is 6.6%).

Due to the small grid size used in this benchmark problem, the CPU time is modest. For example, the 120-time-unit run shown in Figure 4 took less than 1 min of wall-clock time to complete with 1 CPU (all tests shown in this report, unless otherwise noted, were conducted on an Intel Gold 6130 cluster with CPU clock speed of 3.0 GHz and gigabit EDR infiniband connection).

3.2 BP2: Solitary wave on composite beach – analytical solution

This problem was modeled against Revere Beach located approximately 6 miles northeast of Boston in the City of Revere, Massachusetts. A physical model was constructed at the Coastal Engineering Laboratory of the U.S. Army Corps of Engineers, Vicksburg, Mississippi facility. The model beach consists of three piecewise-linear slopes of 1:53, 1:150, and 1:13 from seaward to shoreward with a vertical wall at the shoreline (Figure 6). In the experiments the wave maker was moved to different locations for each of the 3 cases: A, B and C. Here we simply used the measured time series at gauge 4 as the boundary condition for the model. For comparison with the analytical solution, which was derived from the linearized SWE, we will only consider case A for the reason stated below.

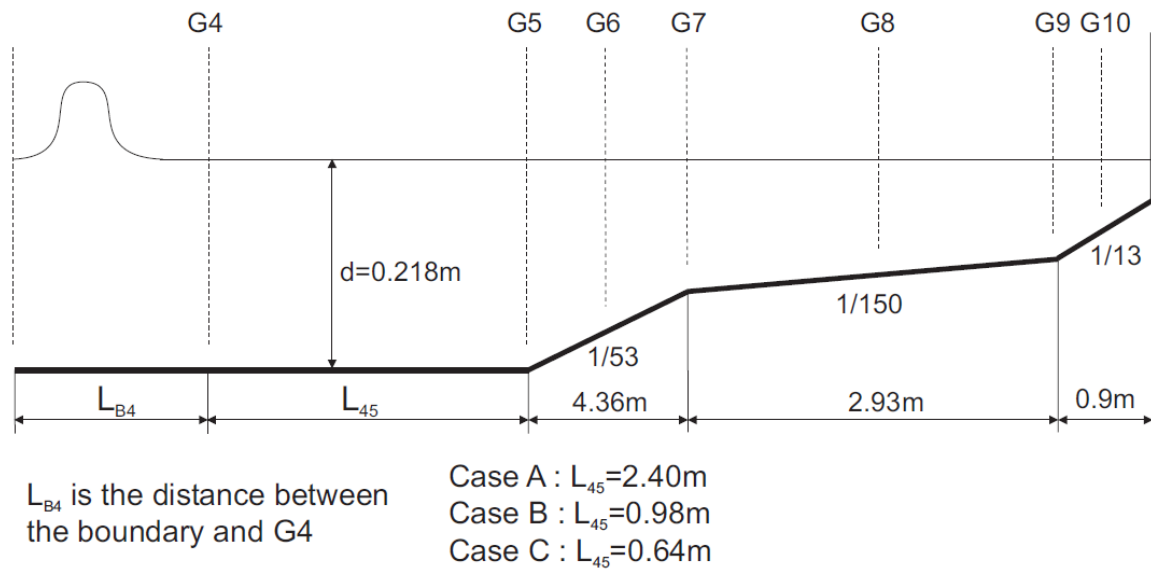


Figure 6 Schematics of the composite beach and locations of gauges used in BP2.

In the model, a rectangular domain with variable grid size ($\Delta y=2.5\text{mm}$ and Δx varies from 1cm at the left boundary to 1mm at the vertical wall, in order to capture the large runup there) was used to cover $12.64\text{m} \leq x \leq 23.23\text{m}$ (case A), $14.06\text{m} \leq x \leq 23.23\text{m}$ (case B) and $14.4\text{m} \leq x \leq 23.23\text{m}$ (case C). Note that we did not use dimensionless variables in this test. The time step was set at 0.05s and the total run time was 30s. The grid for case A was the largest with 11115 nodes, and it took 1 min of wall-clock time to complete the 30-s simulation with 2 CPUs.

Figure 7 shows the comparison at various gauges along the flume. Good agreement is observed in general. The “errors” in the numerical solution can be partly attributed to the different assumptions used in the analytical and numerical solutions; in SCHISM a strict “linear” solution of the SWE is not possible as the flux term in the integrated continuity equation can only be treated nonlinearly.

For the other two cases (B&C), the amplitude of the incident wave is not small as compared to the water depth, and therefore the analytical solution, which linearizes the SWE around $\eta = 0$, is definitely not valid even as a 1st-order approximation of the SWE. Consequently, we excluded these in this section. Comparison with the lab data will be presented in Section 3.4.

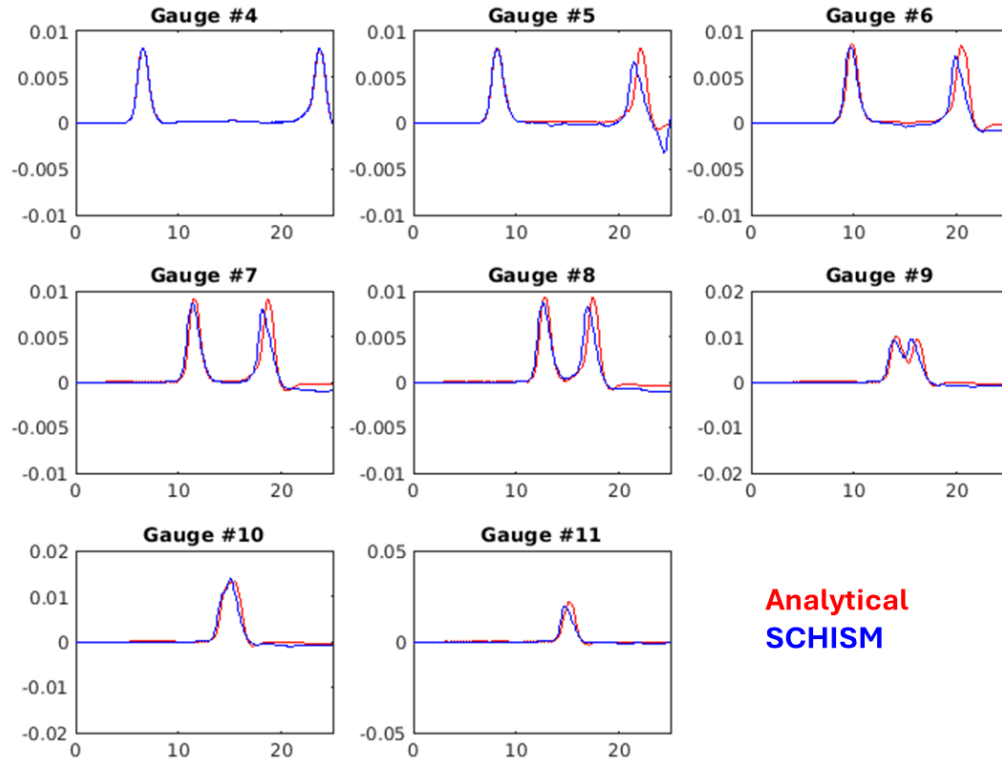


Figure 7 Comparison of elevation time history at 8 stations for case A of BP2. Gauge 4 is located at the domain boundary and serves as a check for the imposed boundary condition; gauge 11 is at the vertical wall, where the RMSE is 1.7mm and the Wilmot skill is 0.95.

3.3 BP4: Solitary wave on simple beach – lab experiments

The description of the problem can be found in Section 3.1. Here we compare the results for cases A and C, as well as for the runup as a function of the incident wave height. The model parameters are the same as in Section 3.1, except that non-zero bottom friction based on the Manning formulation was used. Figure 8 shows surface profiles at various times for the non-breaking case A. The model is able to capture the runup and rundown process well. The model performance for the results in Figure 8 is included in Table 3 and is mostly comparable to SELFE.

For wave breaking case C, the SWE is no longer appropriate, and therefore the hydrostatic version of SCHISM initially gave larger errors (Figure 9). The steepening of the crest as seen in the model results is typical of any hydrostatic model due to lack of energy dissipation. After wave breaking occurs, however, the SWE is able to reasonably simulate the runup process (last panel of Figure 9). The modeled maximum runup is also slightly sensitive to the choice of the bottom friction, and a smaller friction leads to a larger runup.

The repeated experiments using different wave heights provided the runups as a function of the wave height, and the comparison is presented in Figure 10. The experiments indicated that wave breaking initiates when $H/d > 0.045$. The modeled runups are accurate up to this limit and are less accurate beyond it (Figure 10).

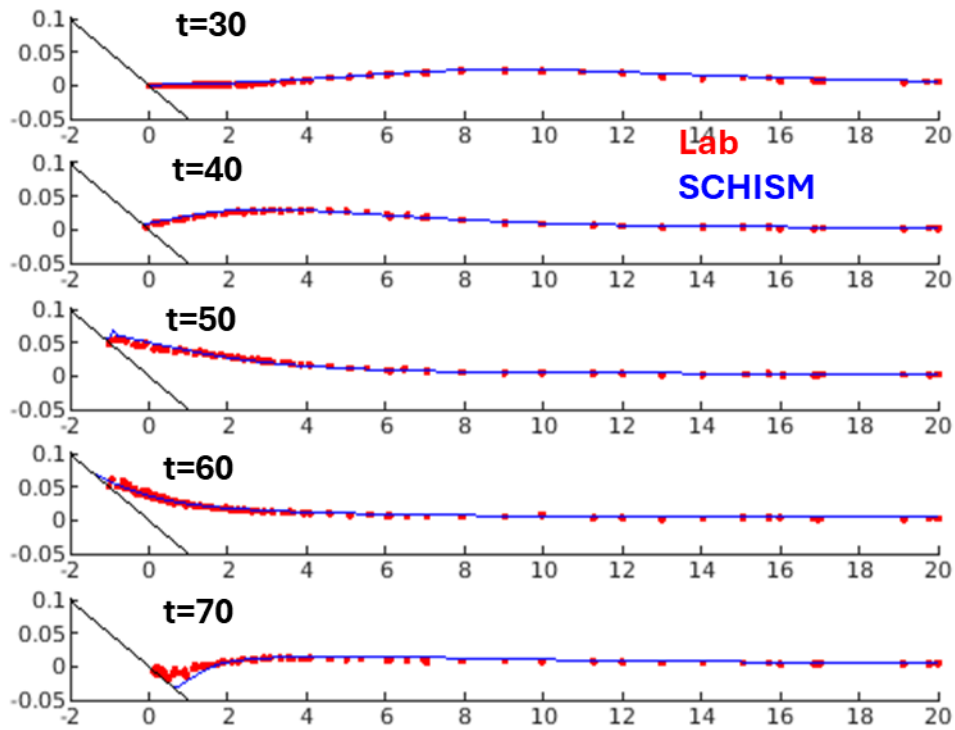


Figure 8 Comparison of surface profiles for case A of BP4. The Manning friction coefficient is $n_0=0.016$. The error for the maximum elevation at $t=60$ (near the maximum runup) is 2%.

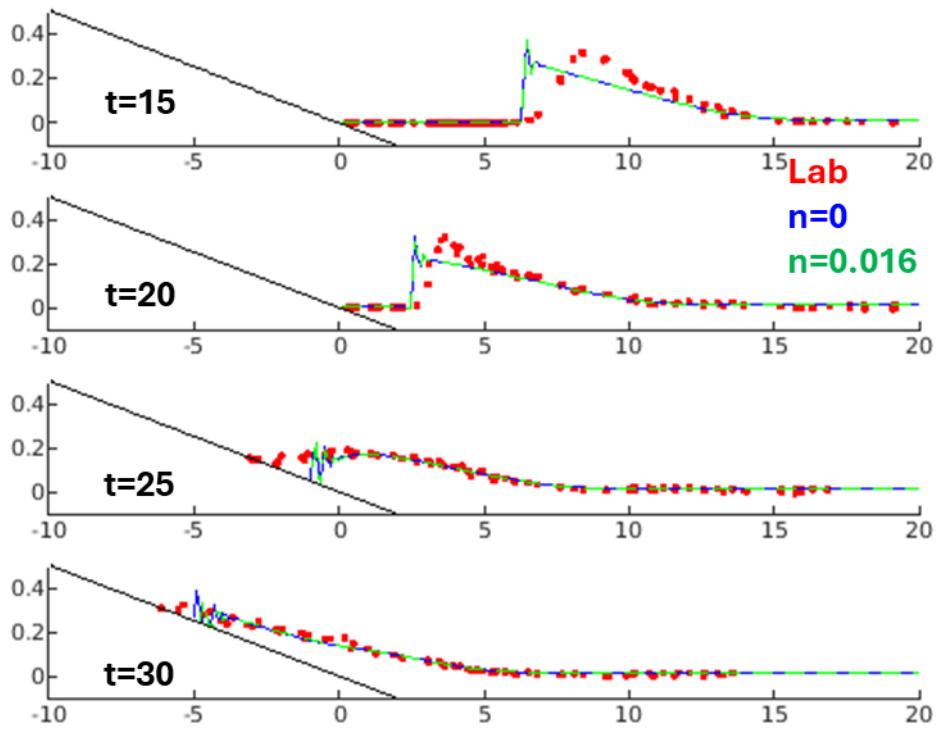


Figure 9 Comparison of surface profiles for breaking-wave case C ($H/d=0.3$) of BP4. Model results with two choices of bottom friction are shown.

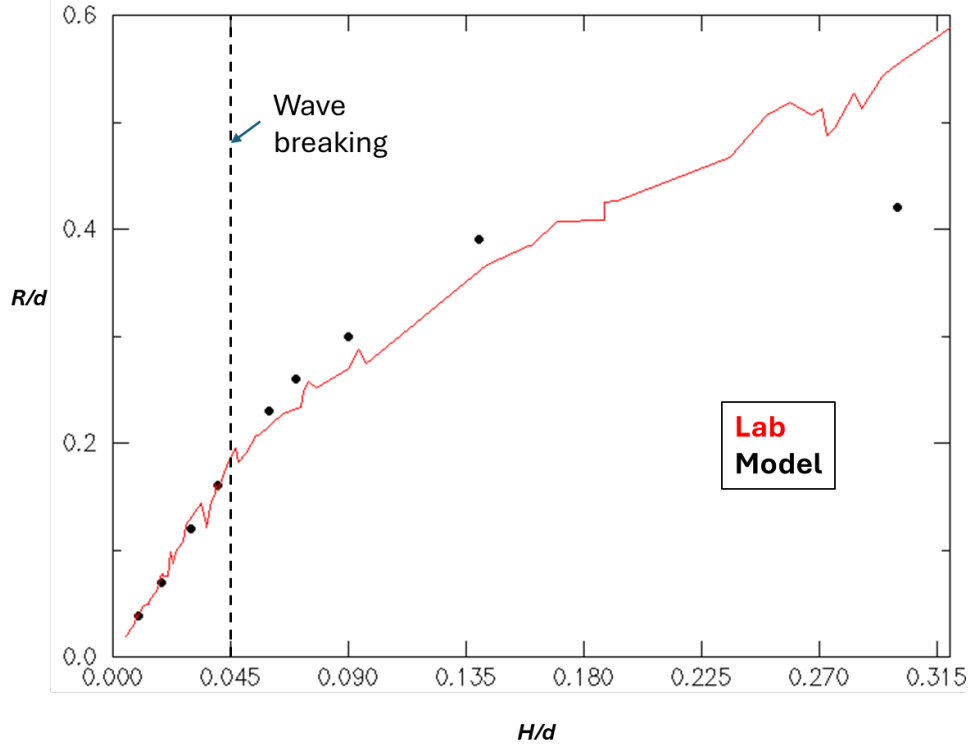


Figure 10 Runups as a function of the incident wave height for BP4. The maximum runup error for non-breaking waves is 5%.

Table 3. BP4 model errors with respect to the lab experiment data a) surface profile for Case A, $H/d = 0.0185$ as simulated by SELFE and SCHISM. 'RMS' is the RMSE normalized by the data range. 'Max' refers to the error for runup error.

Model	t=30		t=40		t=50		t=60		t=70		Mean	
	RMS %	Max %										
SELFE	10	3	9	1	5	3	4	3	14	2	8	2
SCHISM	9	6	8	3	6	12	4	2	14	6	8	6

3.4 BP5: Solitary wave on composite beach – lab experiments

The set-up of the experiments has been described in Section 3.2. The model uses the nonlinear SWE instead of the linear SWE as in Section 3.2. We have also explored variation of the Manning coefficient (n_0) but found little sensitivity in the results to this parameter. The results presented below were obtained using $n_0=0$.

The elevation time series for all 3 cases (A, B and C) are presented in Figures 11-13. The mismatches in the mean water level at gauge 7 in Figure 11 etc. suggest a problem in the lab data. In general, the model results compare reasonably well with the lab data, except for the largest wave of case C (Figure 13).

Furthermore, the modeled runups at the vertical wall are also in reasonable agreement with the data for cases A and C. For case A, the modeled and lab measured runups are 2.5cm and 2.7cm, respectively. For case C, they are 24cm and 27.4cm. For case B, the large waves colliding with the wall generated very high splash which explains the largest runup measured among the 3 cases (45.7cm). Since the model does not explicitly simulate this process, the modeled runup was substantially lower (19cm). The runup results from SCHISM are similar to that from SELFE. In all three cases, the model runs were stable with no sign of instability.

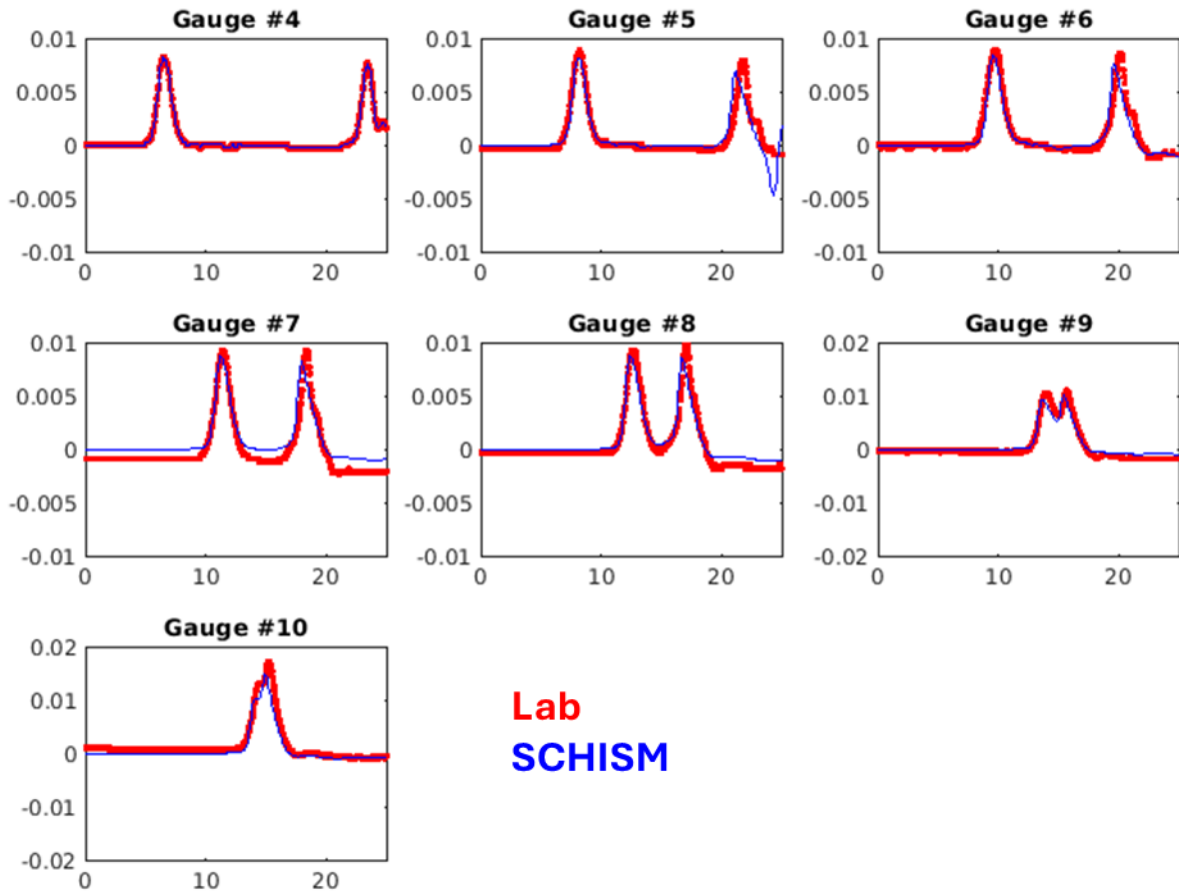


Figure 11 Comparison of elevation time series for case A ($L_{45} = 2.40$ m) of BP5.

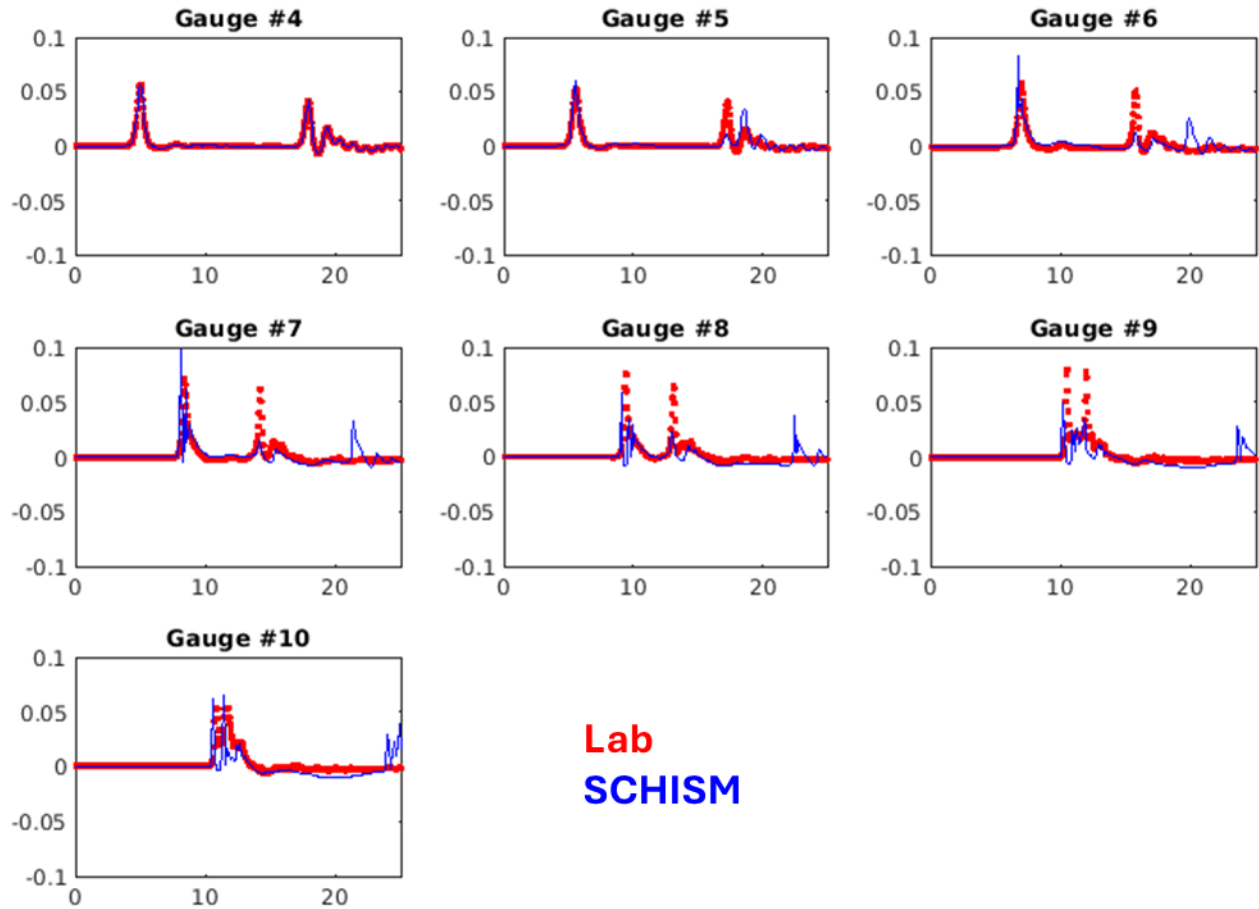


Figure 12 Comparison of elevation time series for case B ($L_{45} = 0.98$ m) of BP5.

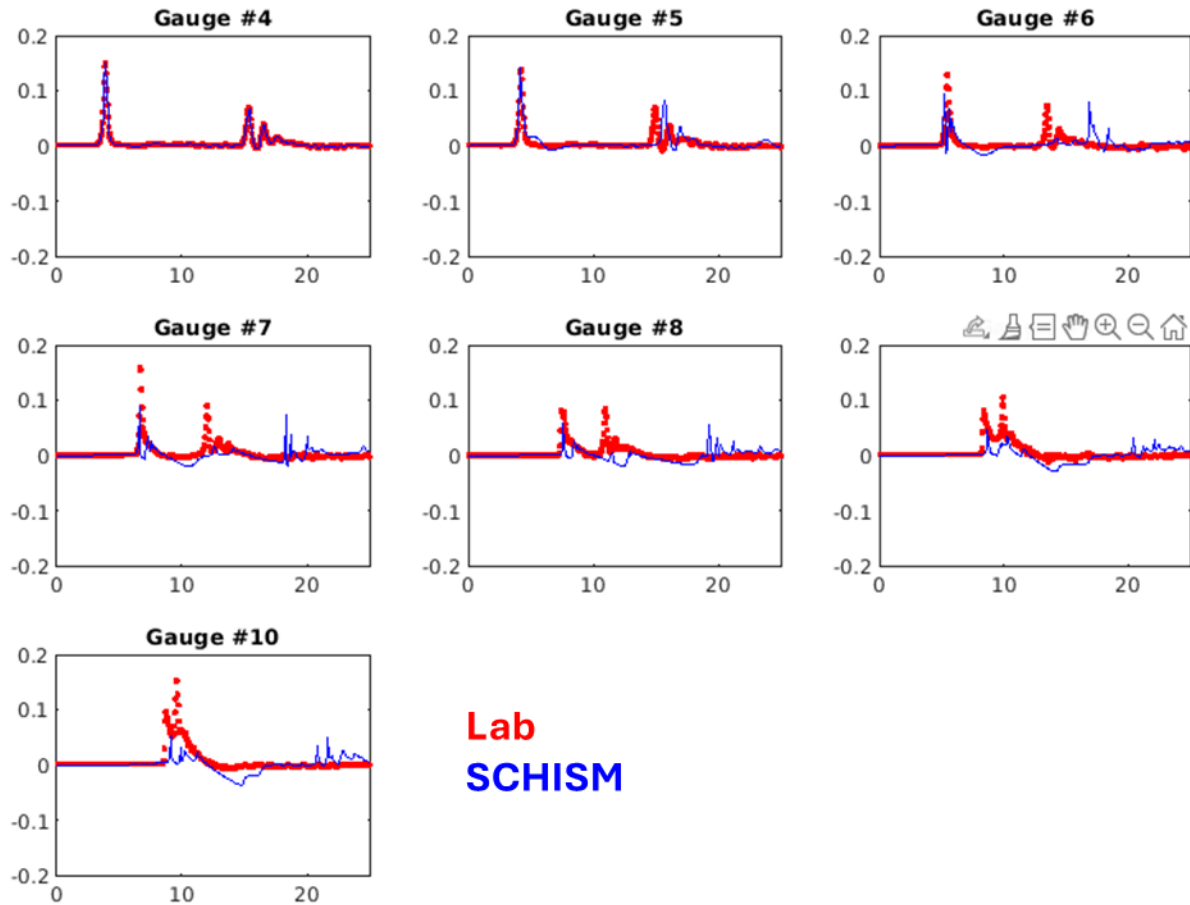


Figure 13 Comparison of elevation time series for case C ($L_{45} = 0.64$ m) of BP5.

3.5 BP6: Solitary wave on a conical island

To examine the model performance in more than one dimension, the experiment of solitary wave around a conical island (Figure 14a) is simulated numerically here. The lab data includes time series at various gauges in the tank as well as run-up measurements around the perimeter of the conical island.

We did not model the wave maker in the experiment but instead used the time series at a gauge close to the wave maker as the boundary condition. An unstructured grid was generated for this problem to better resolve the downwave side of the island where large runups due to collision of two waves were expected. A 10cm grid size was used at the outer tank boundaries, 1cm at the boundary of the flat top of the cone (which has a diameter of 2.2m), and 5cm in the upwave half of the circle that defines the toe of the conical island, and 2cm for the downwave half (Figure 15). The total number of the nodes was 256494 for case A (the largest grid). The time step was set at 0.02s, and the Manning's coefficient $n_0=0.01$. The total simulation time was 60s, which took 4 min of wall-clock time on 32 CPUs.

Figure 14 shows the comparison of elevation time series at 4 gauges (#6, #9, #16 and #22) for 3 cases ($H=0.045$, $H=0.096$, $H=0.181$), with progressively larger incident wave amplitude. The modeled elevations are in good agreement with the lab data and the model was stable for all cases. A summary of error statistics is shown in Table 3.

Table 3. Error statistics for the 3 cases of BP6. RMS is the RMSE normalized by the data range; MAX is the relative error for the maximum runup.

CASE A	Gauge 6		Gauge 9		Gauge 16		Gauge 22		Mean	
	<i>RMS</i> %	<i>Max</i> %								
SELFE	6	2	5	4	8	18	8	7	7	8
SCHISM	5	3	5	1	8	19	8	9	7	8

CASE B	Gauge 6		Gauge 9		Gauge 16		Gauge 22		Mean	
	<i>RMS</i> %	<i>Max</i> %								
SELFE	6	1	7	3	7	10	9	28	7	11
SCHISM	6	0	7	4	7	9	9	27	7	10

CASE C	Gauge 6		Gauge 9		Gauge 16		Gauge 22		Mean	
	<i>RMS</i> %	<i>Max</i> %								
SELFE	6	3	12	13	8	5	8	22	9	11
SCHISM	6	2	10	15	11	3	8	21	9	10

The modeled runup distribution around the island is compared to the measured values in Figure 16, while Figure 17 is a spatial representation of the same information as in Figure 16. The agreement is good for cases A and B; the maximum errors were below 6%. For case C, both lab data and model results exhibit a slight asymmetry (Figure 17) and the model has an underestimation of the maximum runup at the back of the island. The wave breaking that occurred in this case cannot be accurately modeled by SCHISM but the error still falls below the 20% allowable error specified in Table 1-5 (NTHMP, 2012). Comparison of error statistics against SELFE is shown in Table 4.

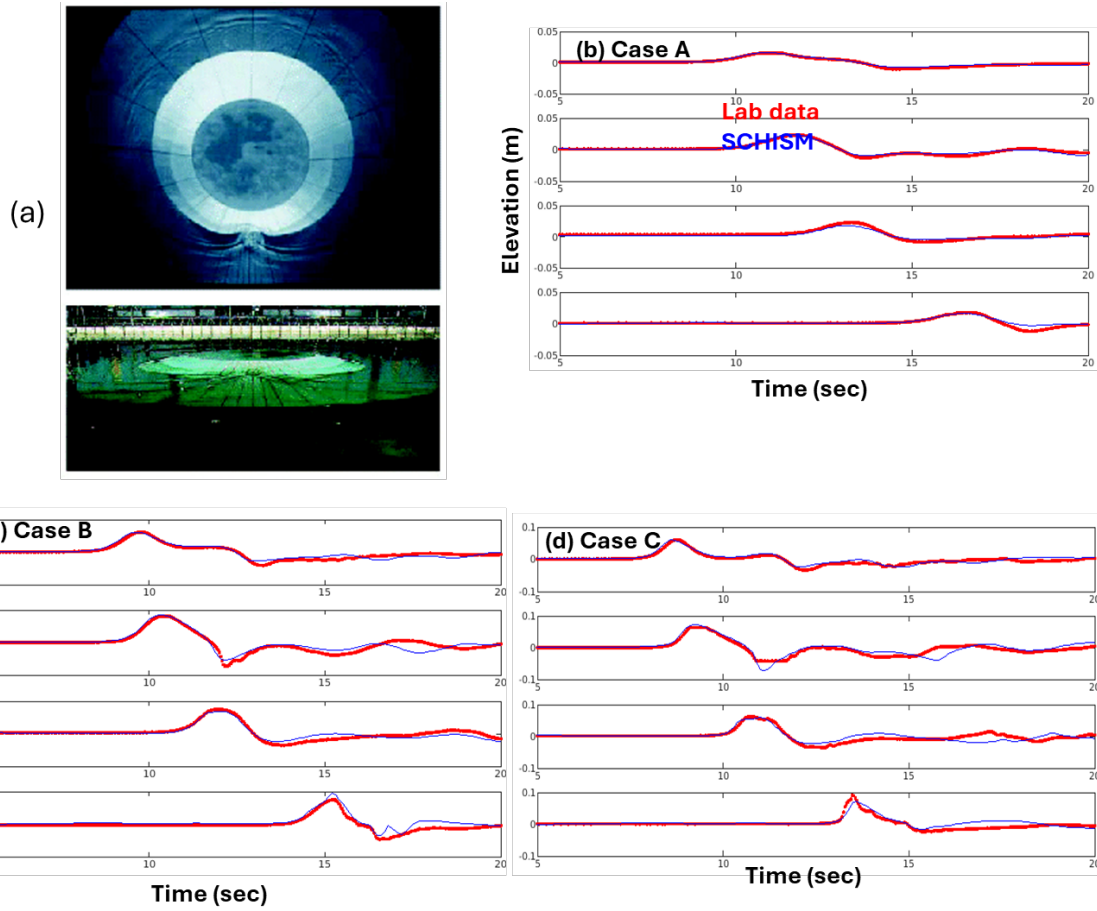


Figure 14 Comparison of elevation time series at 4 gauges for 3 cases of BP6. (a) shows the experimental setup.

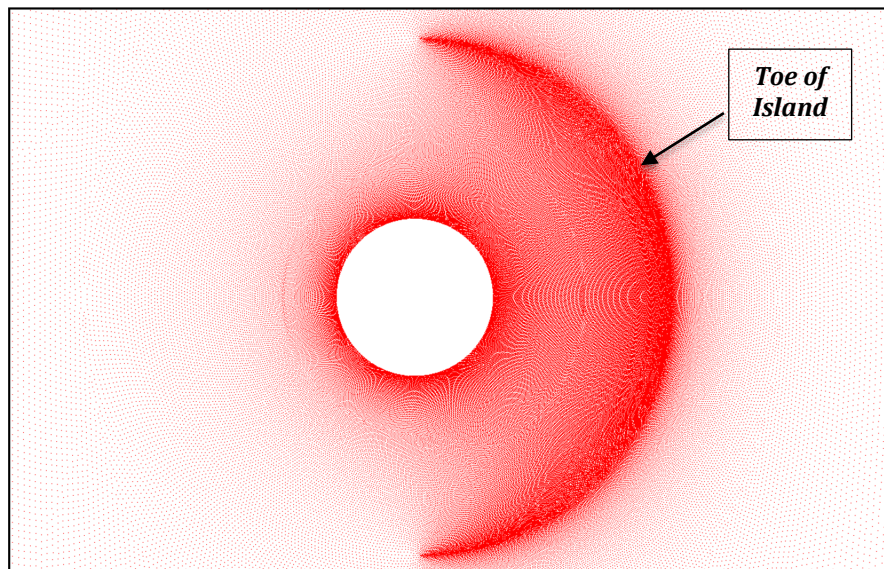


Figure 15 Nodes in the unstructured grid used in BP6.

Table 4. Error statistics for runups for the 3 cases of BP6. RMS is the RMSE normalized by the data range; MAX is the relative error for the maximum.

	Case A		Case B		Case C		Mean	
	RMS %	Max %	RMS %	Max %	RMS %	Max %	RMS %	Max %
SELFE	14	4	11	4	10	2	12	3
SCHISM	13	3	10	4	10	0	11	2

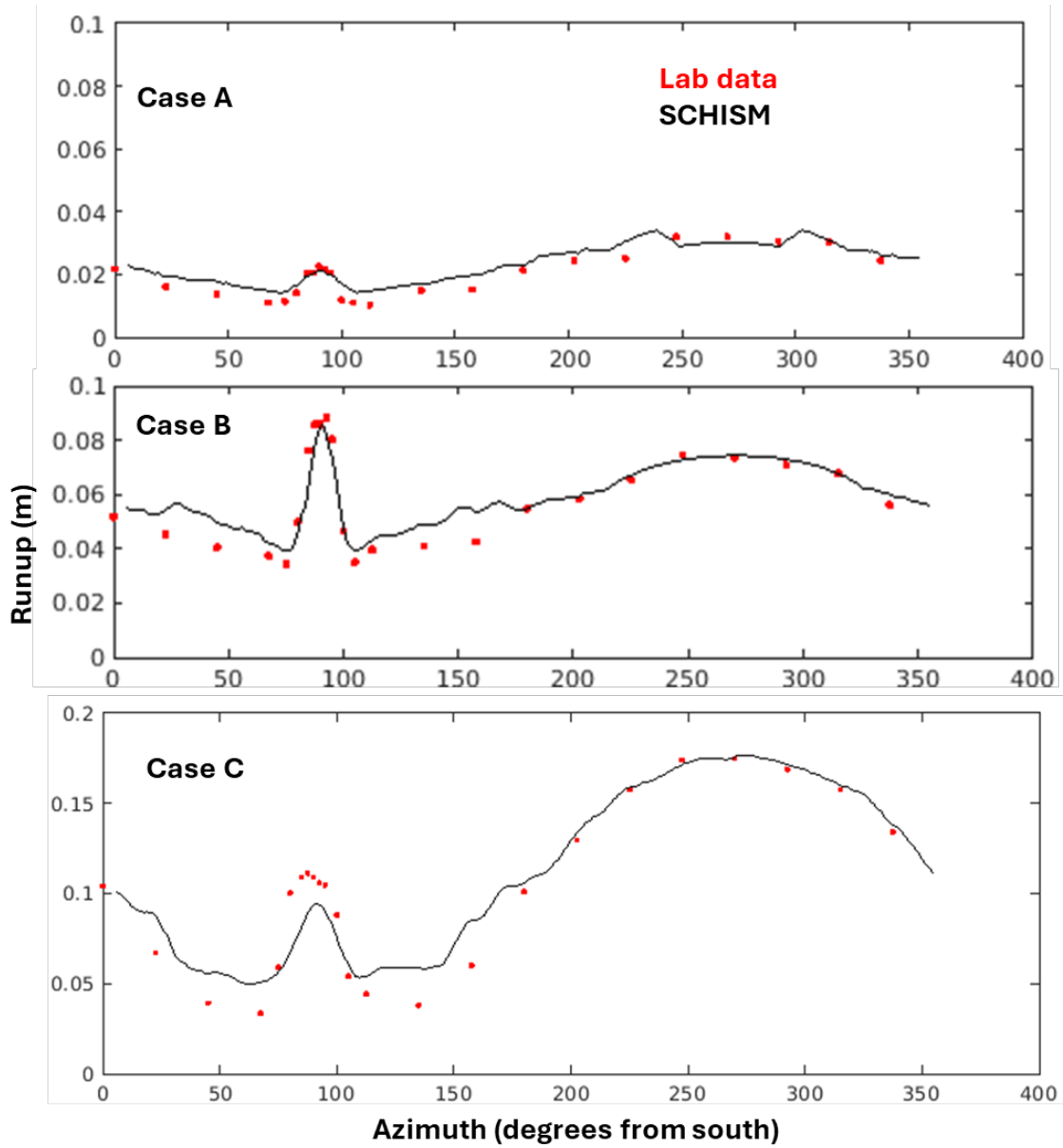


Figure 16 Comparison of runups around the conical island for the 3 cases of BP6.

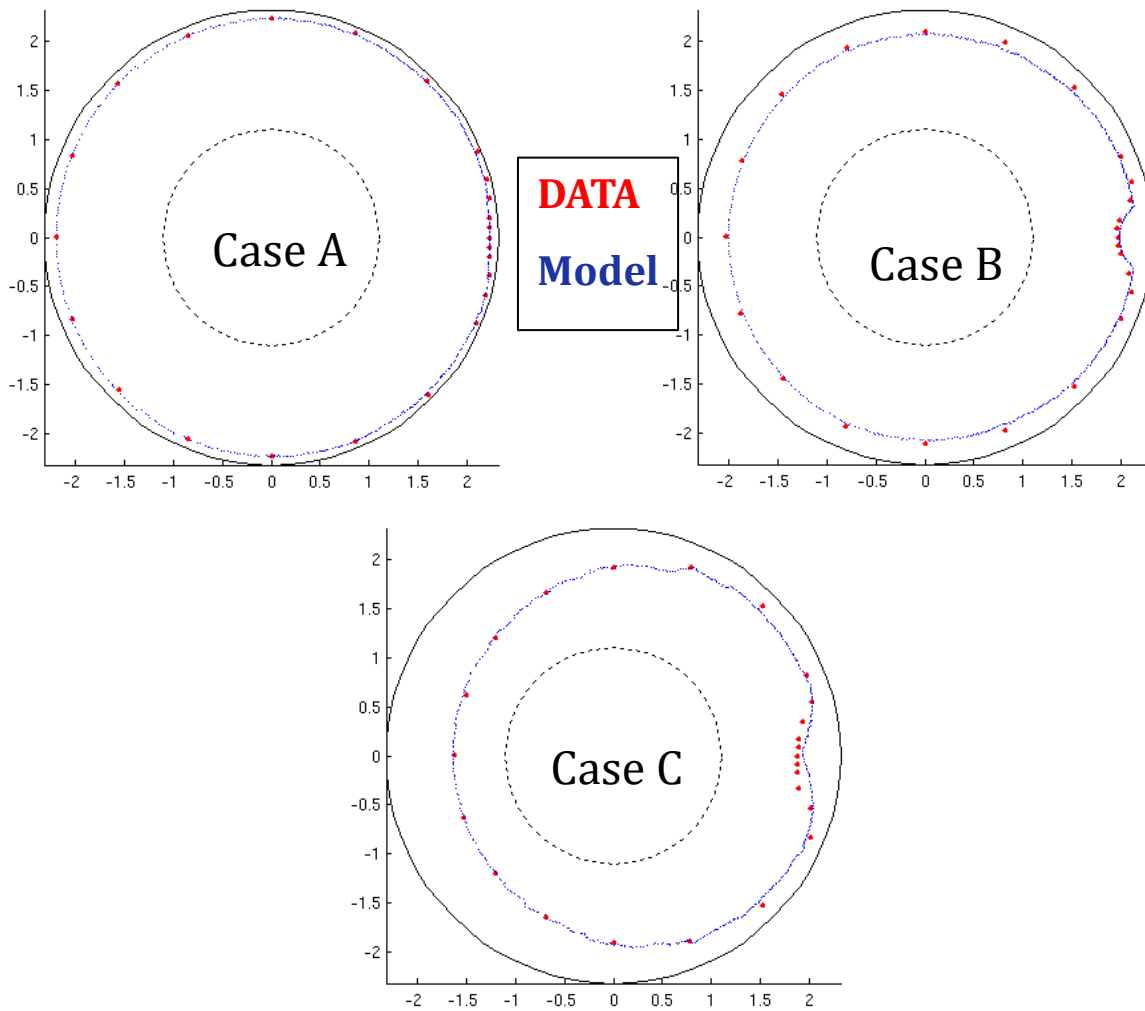


Figure 17 Comparison of runups around the conical island for the 3 cases of BP6, in spatial form.

3.6 BP7: Wave runup on Monai Valley

This test considers the wave tank experiment that models the 1993 Okushiri Island tsunami. The lab data includes time series at 3 gauges (Figure 18a) as well as video images that illustrate the runup sequence in a narrow valley near Monai.

The model used a uniform grid resolution of 1.4cm and a time step of 0.01s. Therefore, there were altogether 95892 nodes in the grid. We have tested the sensitivity to the Manning's n_0 and found little influence from this parameter. The results below were obtained using $n_0=0$. The total simulation time was 22.5s, which took 1 min of wall-clock time with 20 CPUs.

The comparison of time series at the 3 gauges in front of the valley is shown in Figure 18. The model was able to capture the arrival time and the amplitude of the first waves well. The inundation sequence in the narrow valley is shown in Figure 19, which agrees qualitatively with the lab

observation: the modeled maximum runup of 10cm matches the observed mean value of 10cm (and therefore the maximum runup error is 0%).

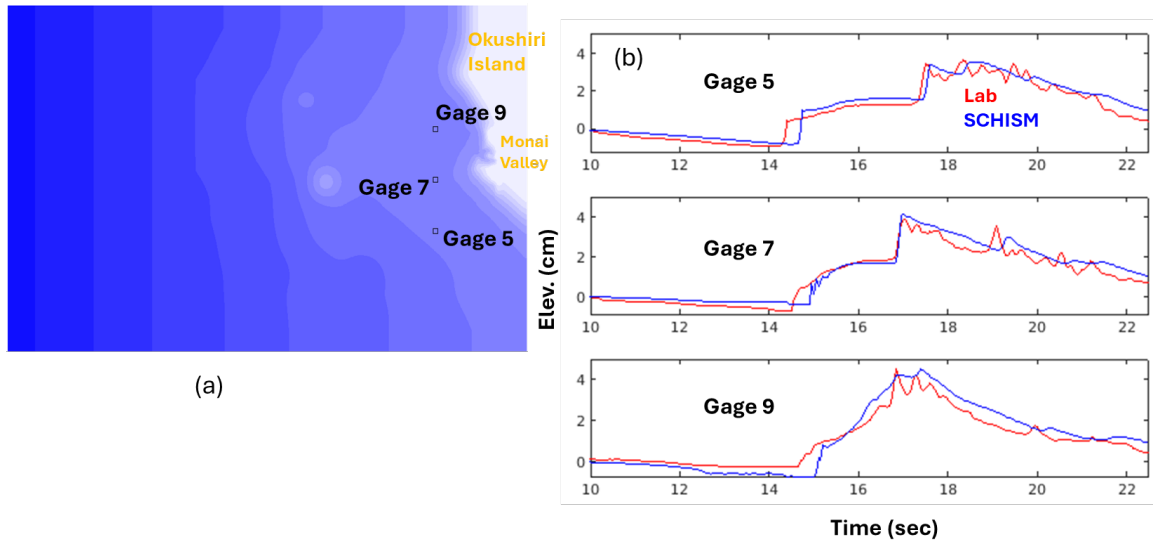


Figure 18 Comparison of elevations at 3 gauges in front of the valley as shown in (a), from BP7. RMSEs for the 3 gauges are 4.2, 3.8 and 4.6 mm, respectively.

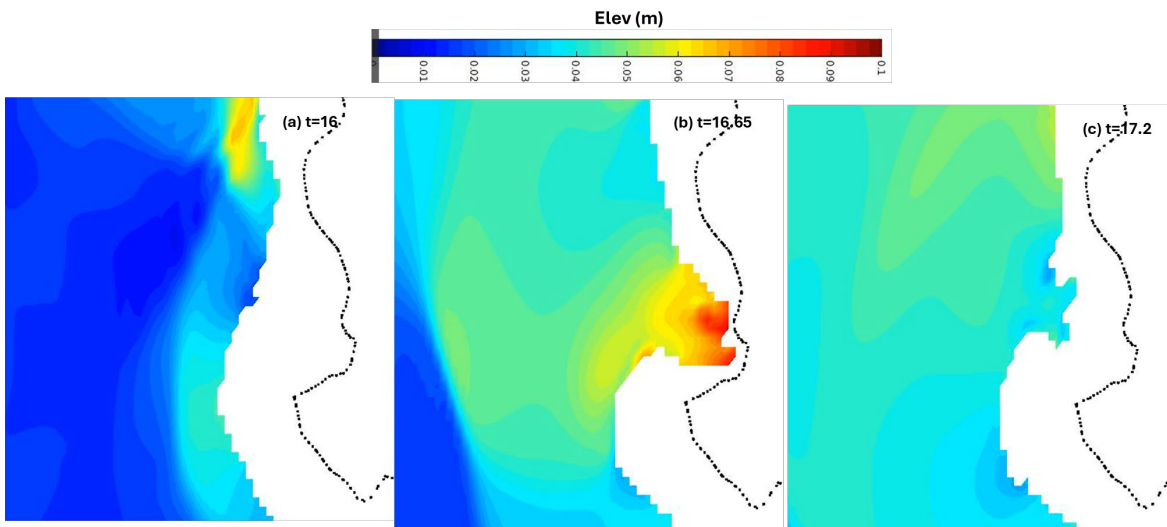


Figure 19 Inundation sequence near the narrow valley in BP7; $t=16.65$ is close to the maximum runup, which is ~ 10 cm. Dash line represents 11cm isobath.

3.7 BP9: Field – Okushiri Island

The first field test conducted was the simulation of the 1993 Hokkaido-Nansei-Oki tsunami that impacted the Japanese island of Okushiri. The historical data were originally collected by the post-tsunami survey group and passed onto the author by Dr. Tomo Takahashi; they include the pre- and post-event bathymetry survey data, the estimated source information, tide gauge records at 2 gauges, and estimated runup distribution around the island. However, the horizontal datum used in the files was later found to contain errors when overlaid with modern maps. The files used in this study were

corrected by Dr. Dmitry Nicolsky (U. Alaska Fairbanks). As shown in Figure 20a, there still appear to be mismatches (offset, indicated by the white arrow) among various files that define the DEMs.

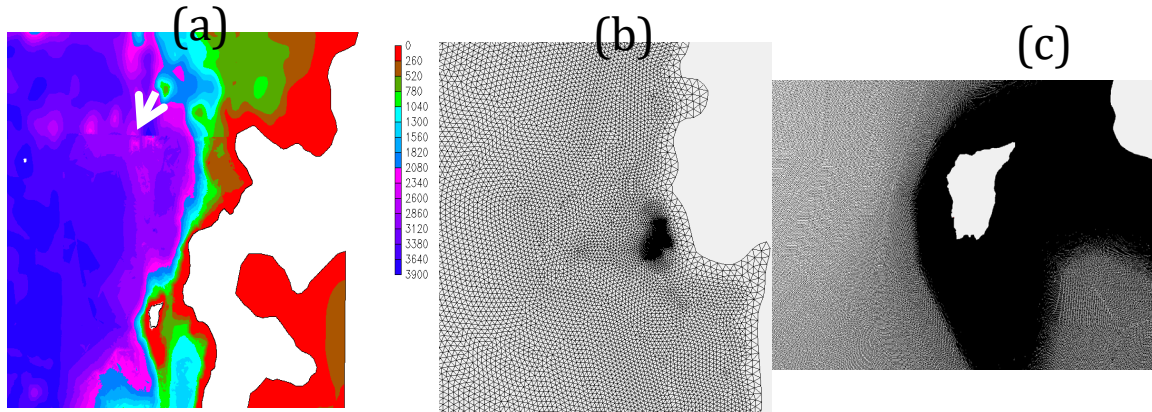


Figure 20 (a) Bathymetry as embedded in DEMs used in BP9; (b) unstructured grid and (c) zoom-in around the Okushiri Island. The white arrow in (a) indicates a mismatch of bathymetry from multiple DEM sources.

To better capture the runup distribution around the island we used variable resolution around the island, with 30m resolution at the shoreline, and ~5m around the narrow Tsuji Valley where the maximum runup (~31m) was observed (Figure 20). At the outer ocean boundary, we used a coarse resolution of 7km. The total number of nodes in the grid was 2544177 with over 95% spent around the island. Note that the original grid used by SELFE was lost, and we had to re-create the grid here for SCHISM. A time step of 0.5s was used to carry out the 1-hour simulation, which took 20 min on 320 CPUs.

The comparison at the 2 tide gauges is shown in Figure 21. While the modeled arrival time approximately matched the gauge record at Esashi, it was too early at Iwanai, suggesting errors in the source information; note that a similar mismatch was also observed by Kato and Tsuji (1994).

On the other hand, the agreement between the model and data for the distribution of the runups around the island was much more reasonable (Figure 22). Note that the data were digitized from a figure in Kato and Tsuji (1994) and therefore the precise locations of observation were unknown. Nevertheless, the model seemed to have captured well the variation along the west, north and south coast, with large errors along the east coast, where the errors in the source information may be more pronounced. The model adequately simulated the large runups around the Tsuji Valley (with 20% error) on the west coast, and around Aonae-Hamatsumae on the south coast. The two waves reported in various post-tsunami surveys as arriving ~10min apart devastated the town of Aonae; these were correctly simulated by the model (Figure 23). Overall, our SCHISM modeling indicates slight improvements, when compared with the SELFE model runup elevations. We believe the difference is most likely due to the different grids used.

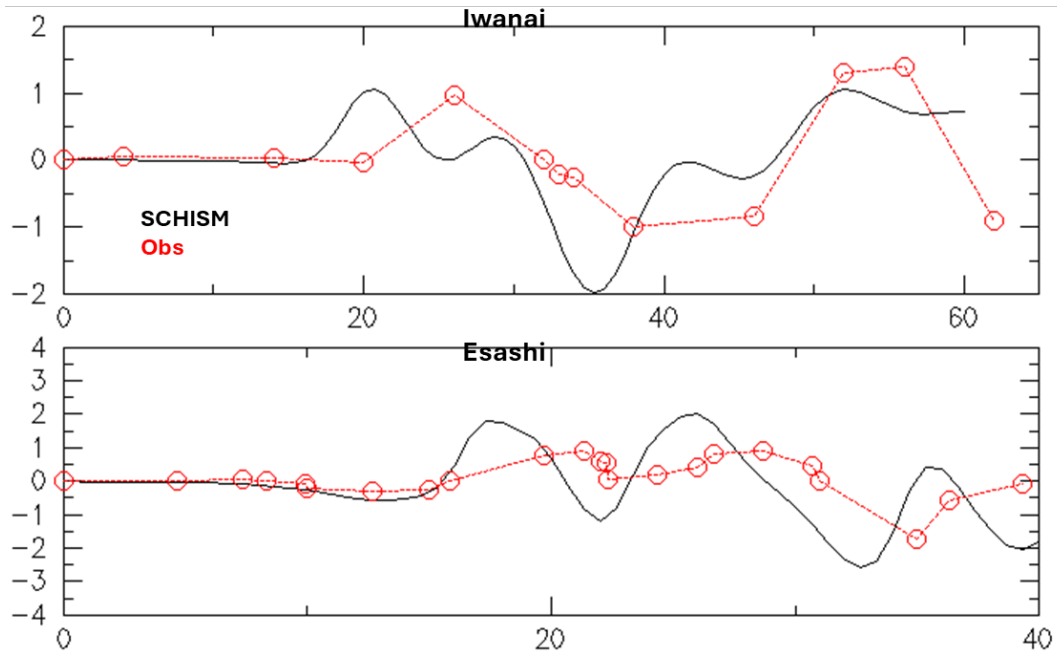


Figure 21 Comparison of elevations at 2 tide gauges in BP9.

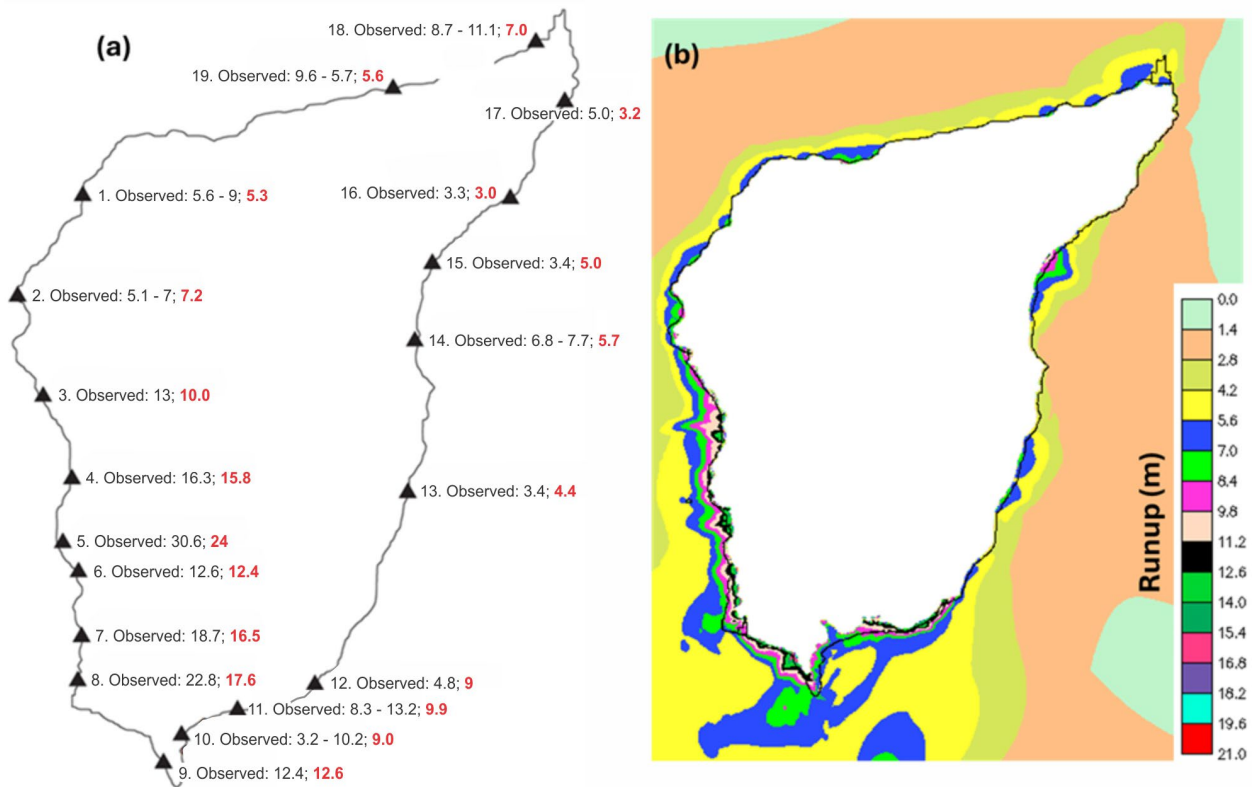


Figure 22 (a) Comparison of runups around the island in BP9. Red numbers are from the model. (b) Model predicted runups around the island. The coordinates given by the file provided by the Workshop have a datum shift so the coordinates used in this plot are from the Workshop final report.

Table 5. Runup errors from SCHISM and SELFE (the latter from NTHMP 2012 report) for BP9. The errors were calculated using the best match if the observation is specified in a range. SCHISM errors show 2 numbers (error in meters and % error in parentheses).

ID	Longitude	Latitude	Observed (m)	SCHISM errors m (%)	SELFE errors (%)
1	139.4292	42.18818	5.6-9.0	-0.3 (5%)	0
2	139.4112	42.16276	5.1-7	0.2 (3%)	11
3	139.4183	42.1374	13	-3 (23%)	58
4	139.4262	42.11655	16.3	-0.5 (3%)	0
5	139.4237	42.10041	30.6	-6.6 (22%)	14
6	139.428	42.09301	12.6	-0.2 (2%)	12
7	139.4289	42.07664	18.7	-2.2 (12%)	5
8	139.4279	42.06546	22.8	-5.2 (22%)	0
9	139.4515	42.0447	12.4	0.2 (1%)	0
10	139.4565	42.05169	3.2-10.2	0	0
11	139.472	42.05809	8.3-13.2	0	0
12	139.4934	42.0645	4.8	4.2 (87%)	71
13	139.5191	42.11306	3.4	1 (29%)	20
14	139.5211	42.15138	6.8-7.7	-1.1 (13%)	58
15	139.5259	42.17101	3.4	1.6 (47%)	13
16	139.5475	42.18745	3.3	-0.3 (6%)	10
17	139.5625	42.21198	5	-1.8 (36%)	41
18	139.5546	42.22698	8.7-11.1	-1.7 (19%)	0
19	139.5151	42.21525	5.7-9.6	-0.1 (2%)	14
		Mean		17	17

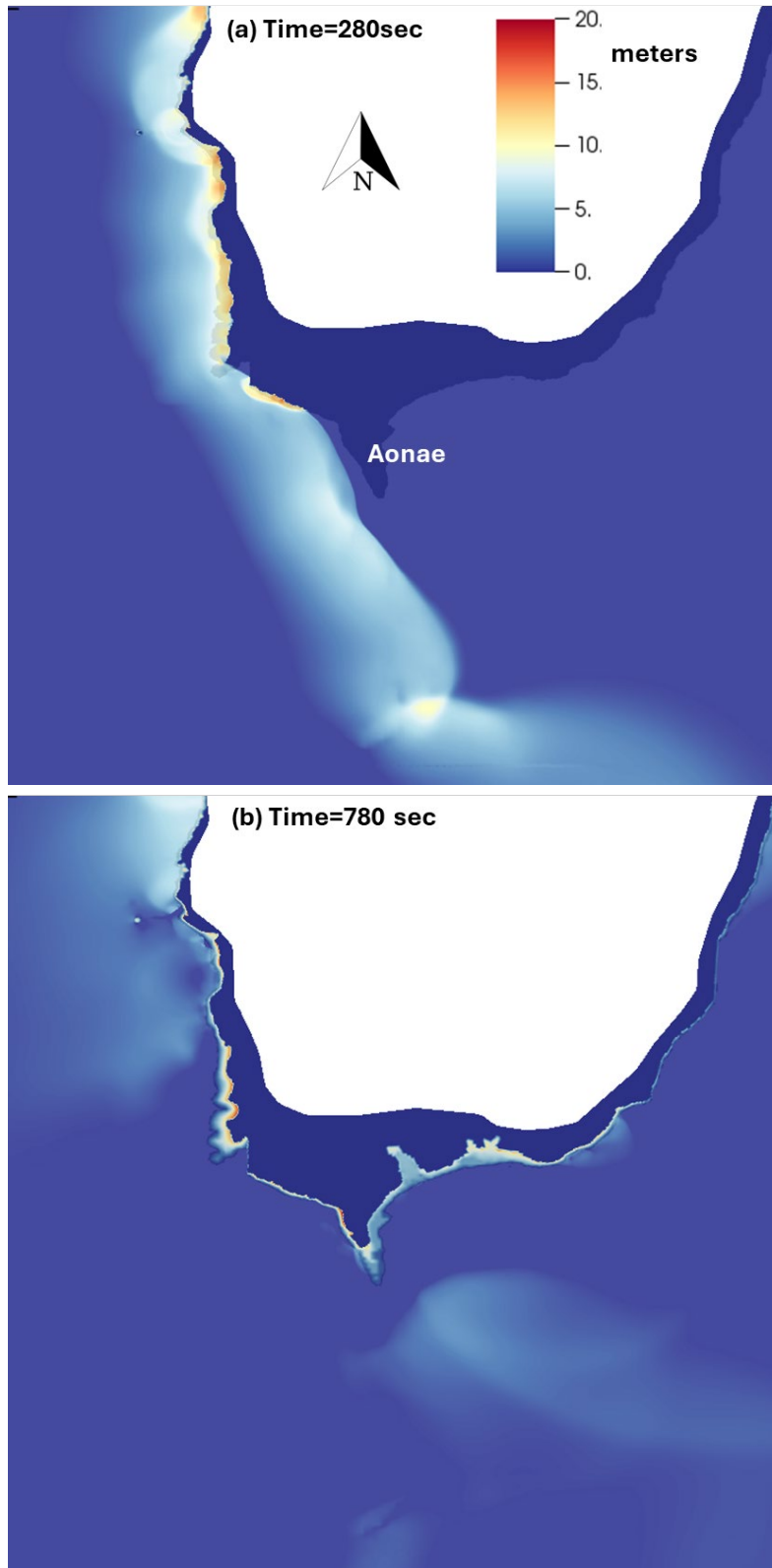


Figure 23 Arrival of 2 waves at Aonae in BP9. The 1st wave came from the west while the 2nd wave attacked from the east.

Lessons learned

During the benchmarking exercise one of the most perplexing problems we have encountered was related to the incomplete information regarding those tests. We had to spend considerable amount of time gleaning files from various sources. For the field test (Okushiri etc) some critical pieces of information (such as the horizontal datums of the DEMs) are still missing. Perhaps the most serious problem with field tests is uncertainty about the geometry of the earthquake source. This issue causes serious errors in simulations for areas proximal to the source (e.g, poor match of simulated runup on the east coast of Okushiri Island).

The set of benchmark problems proposed in OAR-PMEL-135 was found to be mostly appropriate except for a few extreme cases (e.g., the larger wave breaking case C in the composite beach case). The combination of analytical, lab and field tests adequately tests the performance of models.

Additional field tests have been done using SCHISM for the 1964 Great Alaska tsunami, with focus on its impact on the Oregon coast for select ports and harbors, and the results are found in various DOGAMI reports (e.g., Allan et al. 2018, 2020, 2024).

Acknowledgements

We are grateful for review comments provided by Dr. Elena Sulimani (University of Alaska), Dr. Juan Horillo (Texas A&M), and Dr. Randy LeVeque (University of Washington) for their careful review of the report.

References

1. Allan, J.C., Zhang, J., O'Brien, F. and Gabel, L., 2018. Columbia River Tsunami Modeling: Towards Improved Maritime Planning Response. Special Paper 51, Portland, Oregon, 83 pp.
2. Allan, J.C., Zhang, J., O'Brien, F. and Gabel, L., 2020. Coos Bay tsunami modeling: Toward improved maritime planning response. O-20-08, Portland, Oregon, 78 pp.
3. Allan, J.C., Zhang, J. and O'Brien, F., 2021. Tsunami Inundation Modeling Update for the Northern Oregon Coast: Tillamook and Clatsop Counties. O-21-08, Portland, Oregon, 38 pp.
4. Allan, J.C., Zhang, J., O'Brien, F. and Gabel, L., 2024. Brookings tsunami modeling: Toward improved maritime planning response. O-24-03, Portland, Oregon, 79 pp.
5. Azvedo, A., Oliveira, A., Fortunato, A.B. and Bertin, X. (2009) Application of an Eulerian-Lagrangian oil spill modeling system to the Prestige accident: trajectory analysis. *J. Coastal. Res.*, 56, 777-781.
6. Burla, M., Baptista, A.M. Zhang, Y., and Frolov, S. 2010 Seasonal and inter-annual variability of the Columbia River plume: a perspective enabled by multi-year simulation databases. *Journal of Geophysical Research*, **115**, C00B16.
7. Goldfinger, C., Nelson, C.H., Johnson, J.E., Morey, A.E., Gutiérrez-Pastor, J., Karabanov, E., Eriksson, A.T., Gràcia, E., Dunhill, G., Patton, J., Enkin, R., Dallimore, A., and Vallier, T., and the Shipboard Scientific Parties, 2010, Turbidite Event History: Methods and Implications for Holocene Paleoseismicity of the Cascadia Subduction Zone: U.S. Geological Survey Professional Paper 1661-F.
8. Gonzalez F, Geist EL, Jaffe B, Kaˆnogˆlu U, Mofjeld H, Synolakis C, Titov VV, Arcas D, Bellomo D, Carlito, D (2009) Probabilistic tsunami hazard assessment at seaside, Oregon, for near-and far-field seismic sources. *J Geophys Res Oceans* 114: C11023

9. Horrillo, H., Grilli, S.T., Nicolsky, D., Roeber, V. and Zhang, Y. (2014) Performance Benchmarking Tsunami Models for NTHMP's Inundation Mapping Activities, *Pure and Applied Geophysics*, DOI 10.1007/s00024-014-0891-y.
10. Johnson, J., Satake, K., Holdahl, S., Sauber, J. (1996) The 1964 Prince William Sound earthquake: joint inversion of tsunami and geodetic data. *J. Geophys. Res.*, 101(B1), 523–532.
11. Kato, K., and Tsuji, Y. (1995) Estimation of fault parameters of the 1993 Hokkaido-Nansei-Oki earthquake and tsunami characteristics. *Bull. Earthq. Res. Inst.*, Univ. of Tokyo, vol. 69, 39-66.
12. Lynett, P.J., Gately, K., Wilson, R., Montoya, L., Adams, L., Arcas, D., Aytore, B., Bai, Y., Bricker, J.D., Castro, M.J., Cheung, K., David, C., Dogan, G., Escalante, C., Gonzalez, F.I., Gonzalez-Vida, J., Grilli, S.T., Heitmann, T.W., Horrillo, J., KaÄnoÄ,Ä, lu, U., Kian, R., Kirby, J.T., Li, W., Macaas, J., Nicolsky, D.J., Ortega, S., Pampell-Manis, A., Park, Y., Roeber, V., Sharghivand, N., Shelby, M., Shi, F., Tehranir, B., Tolikova, E., Thio, H., Velioglu, D., Yalciner, A., Yamazaki, Y., Zaytsev, A., Zhang, Y. (2017) Inter-Model Analysis of Tsunami-Induced Coastal Currents, *Ocean Modelling*, 114, 14-32 (<http://dx.doi.org/10.1016/j.ocemod.2017.04.003>).
13. NTHMP (2012) Proceedings and results of the 2011 NTHMP (National Tsunami Hazard Mitigation Program) model benchmarking workshop. Boulder: US Depart. of Commerce/NOAA/NTHMP, NOAA Special Report 436p.
14. Pinto, L., Fortunato, A.B., Zhang, Y., Oliveira, A. and Sancho, F.E.P. Development and validation of a three-dimensional morphodynamic modelling system, *Ocean Modelling* (submitted).
15. Priest, G.R., Goldfinger, C., Wang, K., Witter, R.C., Zhang, Y.J., and Baptista, A.M., (2009) Confidence levels for tsunami-inundation limits in northern Oregon inferred from a 10,000-year history of great earthquakes at the Cascadia subduction zone: *Natural Hazards*, DOI 10.1007/s11069-009-9453-5.
16. Priest, G.R., Witter, R.C., Zhang, Y., Wang, K., Goldfinger, C., Stimely, L.L., English, J.T., Pickner, S.G., Hughes, K.L.B., Willie, T.E. and Smith, R.L., 2013. Tsunami inundation scenarios for Oregon. Open file report O-13-19, Oregon Department of Geology and Mineral Industries, Portland, Oregon.
17. Rodrigues, M., Oliveira, A., Queiroga, H., Fortunato, A.B., and Zhang, Y. 2009a Three-Dimensional Modeling of the Lower Trophic Levels in the Ria de Aveiro (Portugal), *Ecological Modelling*, **220**(9-10), 1274-1290.
18. Rodrigues, M., Oliveira, A., Costa, M., Fortunato, A.B. and Zhang, Y. 2009b Sensitivity analysis of an ecological model applied to the Ria de Aveiro. *Journal of Coastal Research*, **SI56**, 448-452.
19. Roland, A., Zhang, Y., Wang, H.V., Maderich, V. and Brovchenko, I. 2011 A fully coupled wave-current model on unstructured grids, *Compt. & Geosciences* (submitted).
20. TPSWG (Tsunami Pilot Study Working Group) (2006) Seaside, Oregon tsunami pilot study—modernization of FEMA flood hazard maps. National Oceanic and Atmospheric Administration OAR Special Report, NOAA/OAR/PMEL, Seattle, WA.
21. Willmott, Cort J.; Ackleson, Steven G.; Davis, Robert E.; Feddema, Johannes J.; Klink, Katherine M.; Legates, David R.; O'Donnell, James; Rowe, Clinton M. (1985) Statistics for the Evaluation and Comparison of Models, *J. Geophys. Res.*, Vol. 90, No. C5, pp. 8995–9005
22. Witter, R.C. (2008) Prehistoric Cascadia tsunami inundation and runoff at Cannon Beach, Clatsop County, Oregon, Oregon Department of Geology and Mineral Industries, Open-File Report O-08-12, 36 p., appendices.
23. Witter, R.C., Jaffe, B., Zhang, Y. and Priest, G.R. (2011) Reconstructing hydrodynamic flow parameters of the 1700 tsunami at Cannon Beach, Oregon, USA., *Natural Hazards*, DOI 10.1007/s11069-011-9912-7.
24. Witter, R.C, Zhang, Y., Wang, K., Goldfinger, C., Priest, G.R., Allan, J.C. (2012) Coseismic slip on the Cascadia megathrust implied by tsunami deposits in an Oregon lake. *Journal of Geophysical Research-Solid Earth*, 117, B10303, doi:10.1029/2012JB009404.

25. Witter, R.C., Y. Zhang, Wang, K., Priest, G.R., Goldfinger, C., Stimely, L., English, J.T. and Ferro, P.A. (2013) Simulated tsunami inundation for a range of Cascadia megathrust earthquake scenarios at Bandon, Oregon, USA, *Geosphere*, 9, 1783-1803.
26. Ye, F., Zhang, Y., Yu, H., Sun, W., Moghimi, S., Myers, E.P., Nunez, K., Zhang, R., Wang, H.V., Roland, A., Martins, K., Bertin, X., Du, J., and Liu, Z. (2020) Simulating storm surge and compound flooding events with a creek-to-ocean model: importance of baroclinic effects, *Ocean Modelling*, 145. <https://doi.org/10.1016/j.ocemod.2019.101526>
27. Zhang, Y., and Baptista, A.M. 2008a SELFE: A semi-implicit Eulerian-Lagrangian finite-element model for cross-scale ocean circulation. *Ocean Modelling*, 21(3-4), 71-96.
28. Zhang, Y., and Baptista, A.M. 2008b An Efficient and Robust Tsunami Model on Unstructured Grids. Part I: Inundation Benchmarks. *Pure and Applied Geophysics*, **165**, 2229–2248.
29. Zhang, Y., Witter, R.W. and Priest, G.P. (2011a) Nonlinear Tsunami-Tide Interaction in 1964 Prince William Sound Tsunami, *Ocean Modelling* 40, 246-259.
30. Zhang, Y. (2011b) Report on benchmark results from SELFE, NTHMP Workshop, Boulder, CO.
31. Zhang, Y., Ye, F., Stanev, E.V., Grashorn, S. (2016). Seamless cross-scale modeling with SCHISM, *Ocean Modelling*, 102, 64-81. doi:10.1016/j.ocemod.2016.05.002